Numerical analysis of mixing enhancement for micro-electroosmotic flow

G. H. Tang,[a] Y. L. He, and W. Q. Tao
State Key Laboratory of Multiphase Flow, School of Energy and Power Engineering, Xi'an Jiaotong University, Xi'an 710049, People's Republic of China

(Received 26 November 2009; accepted 15 March 2010; published online 25 May 2010)

Micro-electroosmotic flow is usually slow with negligible inertial effects and diffusion-based mixing can be problematic. To gain an improved understanding of electroosmotic mixing in microchannels, a numerical study has been carried out for channels patterned with wall blocks, and channels patterned with heterogeneous surfaces. The lattice Boltzmann method has been employed to obtain the external electric field, electric potential distribution in the electrolyte, the flow field, and the species concentration distribution within the same framework. The simulation results show that wall blocks and heterogeneous surfaces can significantly disturb the streamlines by fluid folding and stretching leading to apparently substantial improvements in mixing. However, the results show that the introduction of such features can substantially reduce the mass flow rate and thus effectively prolongs the available mixing time when the flow passes through the channel. This is a non-negligible factor on the effectiveness of the observed improvements in mixing efficiency. Compared with the heterogeneous surface distribution, the wall block cases can achieve more effective enhancement in the same mixing time. In addition, the field synergy theory is extended to analyze the mixing enhancement in electroosmotic flow. The distribution of the local synergy angle in the channel aids to evaluate the effectiveness of enhancement method. © *2010 American Institute of Physics*. [doi:10.1063/1.3391617]

I. INTRODUCTION

The benefits of miniaturization are well established and offer many advantages over conventional macroscopic devices, including compactness, disposability, increased functionality, and enhanced sensitivity. Moreover, microfluidic systems can offer additional benefits such as substantial reductions in reagent consumption and sample volumes, shorter analysis times, and the possibility of *in situ* or point-of-care diagnoses. However, microdevices often behave differently from their macroscale counterparts and it is important to understand the physics at these reduced length scales. One area, in particular, where a better understanding of microfluidic transport processes is important is in the design and optimization of devices that make use of electrokinetic phenomena.

Electroosmosis is a preferred pumping method for microfluidic systems because it involves no moving components. Instead, electroosmosis involves the application of external electric fields to create the fluidic transport. Unfortunately, electroosmotic flow (EOF) is limited to low Reynolds numbers and therefore efficient mixing becomes problematic due to negligible inertial effects. As a consequence, species mixing in EOF is inherently diffusion dominated, requiring either a long mixing channel or a low flow rate to ensure sufficient residence time to achieve a homogeneous solution. To enhance mixing, one approach is to use mechanical methods such as microstirrers.[1,2] However, in addition to increased fabrication costs, mechanical mixing can be undesirable for practical applications because of the moving components. Another approach to enhance mixing is the use of peristaltic or periodic motion in a closed cavity,[3] but these approaches still require some form of mechanical motion.

A variety of methods that avoid the use of moving components have been developed for enhancing the mixing in EOF. For passive micromixers, which do not rely on external stimulation, the main approaches are using a nonuniform zeta potential on the surface of the channel,[4–11] or using microchannels with rough walls or grooved surfaces.[5,12–14] To optimize device design and operation, we need a quantitative understanding of how wall roughness and nonuniform zeta potentials can enhance mixing. Most of previous studies have usually focused on the mixing efficiency since this is one of the most important parameters for evaluating the effectiveness of different mixing enhancement methods. The present study revisits some of the commonly employed mixing enhancement methods and focuses on the degree of mixing and the mixing time. This insight will aid the optimization of EOF-induced mixing and lead to improved device designs while minimizing the need for costly trial-and-error experimentation. In addition, we extend the field synergy theory, which is originally used in enhanced heat transfer field, to analyze the local effectiveness in the channel for various diffusion mixing enhancement methods.

II. NUMERICAL METHODS

The development of the lattice Boltzmann (LB) method has provided a useful alternative simulation approach to computational fluid dynamics.[15,16] As a derivative of lattice gas automata, the LB method differs from traditional numerical approaches which solve the conventional macroscopic governing equations for conserved quantities. Instead, the LB approach tracks the evolution of a distribution function

[a]Electronic mail: ghtang@mail.xjtu.edu.cn.

of the computational particles to describe the conserved fields. This provides an efficient method for obtaining streaming patterns in complicated systems. Recently, the LB method has successfully been applied to simulate the flow fields of a range of electroosmotic applications.[17–26] In the present paper, in addition to describing the flow field, the same LB methodology is also used to simulate the external electric field, the electric potential distribution and species concentration field. One benefit of solving all the fields in the same framework of LB is the ease of programming. Especially this feature could be more useful for a multiprocessor code in parallel computing applications compared with so-called hybrid LB methods.[21]

A. The discrete LB equation

The LB method simulates transport phenomena by tracking the movement of molecular ensembles through the evolution of a distribution function. The discrete LB equation with the Bhatnagar–Gross–Krook collision approximation, including an external force term, can be written as a general form[27]

$$f_i(\mathbf{r}+\mathbf{c}_i\delta_t,t+\delta_t)=f_i(\mathbf{r},t)-\frac{\delta_t}{\tau}[f_i(\mathbf{r},t)-f_i^{eq}(\mathbf{r},t)]+A_i, \quad (1)$$

where f is the distribution function, τ is the relaxation time, $\mathbf{c}_i$ is the particle discrete velocity, δ_t is the lattice time step, and A_i is a substitution term representing the external force. For a D2Q9 square lattice, the discrete particle velocities can be written as $\mathbf{c}_0=0$ (the zero velocity distribution), $\mathbf{c}_i=\{\cos[(i-1)\pi/2],\sin[(i-1)\pi/2]\}c$ for $i=1,2,3,4$ and $\mathbf{c}_i=\{\cos[(i-5)\pi/2+\pi/4],\sin[(i-5)\pi/2+\pi/4]\}\sqrt{2}c$ for $i=5,6,7,8$, where $c=\delta_x/\delta_t$ is the particle streaming speed satisfying $c=\sqrt{3RT}$ and δ_x is the lattice spacing step.

In Eq. (1), $f_i^{eq}(i=0,1,\ldots 8)$ represents the equilibrium distribution function, which for a D2Q9 lattice can be given by a general form $f_i^{eq}=\omega_i B_i$, where B_i is a substitution parameter and the weighing coefficient $\omega_0=4/9$, $\omega_i=1/9$ for $i=1$, 2, 3, and 4 and $\omega_i=1/36$ for $i=5$, 6, 7, and 8. Hence all the adjustment is in the substitution term A_i and substitution coefficient B_i.

1. The flow field

For the flow field, we have the substitution term

$$A_i=\delta_t\frac{\mathbf{F}\cdot(\mathbf{c}_i-\mathbf{u})}{RT}f_i^{eq}(\mathbf{r},t), \quad (2)$$

where $\mathbf{u}$ is the macroscopic velocity, T is the temperature, R is the gas constant, and $\mathbf{F}$ is the external force acting per unit mass, and[28]

$$B_i=\rho\left[1+\frac{3(\mathbf{c}_i\cdot\mathbf{u})}{c^2}+\frac{9(\mathbf{c}_i\cdot\mathbf{u})^2}{2c^4}-\frac{3(\mathbf{u}\cdot\mathbf{u})}{2c^2}\right]. \quad (3)$$

The macroscopic variables such as mass density and momentum density can be obtained by summing over the distribution function, $f_i(\mathbf{r},t)$ i.e.,

$$\rho=\sum_i f_i \quad \text{and} \quad \rho\mathbf{u}=\sum_i f_i\mathbf{c}_i. \quad (4)$$

The kinematic viscosity, ν, is given by

$$\nu=\frac{\tau-0.5\delta_t}{3}\frac{\delta_x^2}{\delta_t^2}. \quad (5)$$

Using the Chapman–Enskog approximation, it can be shown that Eq. (1) recovers the momentum conservation expression in the Navier–Stokes equations

$$\rho\left[\frac{\partial\mathbf{u}}{\partial t}+(\mathbf{u}\cdot\nabla)\mathbf{u}\right]=-\nabla p+\rho\nu\nabla^2\mathbf{u}+\rho\mathbf{F}, \quad (6)$$

where p is the pressure. In the present study, $\rho\mathbf{F}$ is the electrical force acting on the fluid, which is related to the electric potential, Φ by $\rho\mathbf{F}=-\rho_e\nabla\Phi$ where ρ_e is the electric charge density.

2. The electric potential

According to electrostatic theory, the electric potential is described by the following Poisson equation:

$$\nabla^2\Phi=-\frac{\rho_e}{\varepsilon\varepsilon_0}, \quad (7)$$

where ε_0 is the permittivity of free space and ε is the relative dielectric constant of the solution. In general, the electric potential, Φ, can be decomposed into a potential due to the external electric field, ϕ, and a potential due to the electric double layer (EDL), ψ, i.e., $\Phi=\phi+\psi$.[29] Therefore, Eq. (7) can be rewritten as

$$\nabla^2\phi=0, \quad (8)$$

and

$$\nabla^2\psi=-\frac{\rho_e}{\varepsilon\varepsilon_0}. \quad (9)$$

Assuming that the equilibrium Boltzmann distribution is applicable, the net charge density distribution can be expressed as the sum of all the ions in the solution

$$\rho_e=\sum_\alpha z_\alpha e n_{\alpha,\text{inf}}\exp\left(-\frac{z_\alpha e\psi}{k_\text{B}T}\right), \quad (10)$$

where z_α and $n_{\alpha,\text{inf}}$ are the valence and the bulk ionic concentration of type α ions, respectively. The bulk ionic concentration, n_{inf}, can be expressed as the product of the ionic molar concentration, c_{inf}, and Avogadro's number, N_A. The constant, e, is the charge of a proton, and k_B is Boltzmann's constant. Substituting Eq. (10) into Eq. (9) yields the nonlinear Poisson–Boltzmann equation

$$\nabla^2\psi+\frac{1}{\varepsilon\varepsilon_0}\sum_\alpha z_\alpha e n_{\alpha,\text{inf}}\exp\left(-\frac{z_\alpha e\psi}{k_\text{B}T}\right)=0. \quad (11)$$

If a uniform dielectric constant is assumed and any fluctuations in the dielectric constant are neglected [since the ion-convection effect is insignificant compared to ion diffusion when the Peclet number is less than 100 (Ref. 30)], then the net charge density distribution in a symmetric electrolyte is

proportional to the concentration difference between the cations and anions, and can be written as[31]

$$n_{\pm} = n_{\text{inf}} \exp\left(\mp \frac{ze\psi}{k_B T}\right), \tag{12}$$

$$\rho_e = ze(n_+ - n_-) = -2zen_{\text{inf}} \sinh\left(\frac{ze\psi}{k_B T}\right). \tag{13}$$

When $ze\psi/k_BT$ is small, Eq. (13) can be linearized and this approximation has been used in many previous simulations. However, in the present paper, we also use the LB Eq. (1) for the evolution of the electric potential due to the EDL with

$$A_i = \delta_t \left[\frac{1}{\varepsilon\varepsilon_0}\sum_{\alpha} z_\alpha e n_{\alpha,\text{inf}} \exp\left(-\frac{z_\alpha e\psi}{k_B T}\right)\right]\omega_i, \tag{14}$$

and $B_i=\psi$. The potential diffusivity, χ, which is equal to unity in the simulations, is defined as

$$\chi = \frac{\tau - 0.5\delta_t}{3}\frac{\delta_x^2}{\delta_t^2}. \tag{15}$$

The macroscopic electric potential in the liquid is calculated from

$$\psi = \sum_i f_i. \tag{16}$$

3. The external electric field

Conventional differential methods have usually been used in previous studies[24] to obtain the externally-applied electric field ϕ governed by Eq. (8). In the present study, the LB method is used in a similar manner for the electric potential in Eq. (9) due to the double layer, ψ detailed in Sec. II A 2. Obviously, Eq. (8) is more convenient to solve without the electric charge density term compared with Eq. (9). We have $A_i=0$ and $B_i=\phi$. Here the relaxation time is calculated similarly to Eq. (15). The macroscopic external electric field is obtained from

$$\phi = \sum_i f_i. \tag{17}$$

4. The species concentration field

In general, a species is transported by convection of the carrier fluid and diffusion due to the concentration gradient. Again, we apply the LB method to describe the species transport in the solute. We have $A_i=0$ and

$$B_i = c_d\left[1 + \frac{3(\mathbf{c}_i\cdot\mathbf{u})}{c^2} + \frac{9(\mathbf{c}_i\cdot\mathbf{u})^2}{2c^4} - \frac{3(\mathbf{u}\cdot\mathbf{u})}{2c^2}\right]. \tag{18}$$

The species concentration c_d is obtained by summing over the appropriate distribution function, i.e.,

$$c_d = \sum_i f_i. \tag{19}$$

Again, applying the Chapman–Enskog expansion, it can be shown that the LB equation for species transport recovers the normal continuum equation for convection and diffusion[32]

$$\frac{\partial c_d}{\partial t} + (\mathbf{u}\cdot\nabla)c_d = D\nabla^2 c_d, \tag{20}$$

where the diffusion coefficient, D, is related to the corresponding relaxation time via

$$D = \frac{\tau - 0.5\delta_t}{3}\frac{\delta_x^2}{\delta_t^2}. \tag{21}$$

Note that the LB equations with the general form of Eq. (1) for external electric field, electric potential distribution in the electrolyte, the flow field, and the species concentration are not coupled together in the present study, and hence δ_t, c, and τ are adjusted independently in different cases. Though we can employ more sophisticated methods, such as conventional finite-volume or finite-difference numerical methods to solve the Poisson–Boltzmann equation or diffusion equation, the convergence of the present LB is efficient for the Poisson–Boltzmann equation and diffusion equation. The iterative computation reaches a local equilibrium within a short time and can be terminated independently. Coding all equations in the same LB framework is of great potential especially for multiprocessor computing.

B. Boundary conditions for the LB equation

Boundary conditions can readily be implemented in the LB method, making it an ideal simulation tool for fluid flows in complex geometries. To solve the LB equation for the external electric field ϕ, the values of ϕ at the channel inlet and outlet are fixed. Neumann boundary conditions (with $\partial\phi/\partial\mathbf{n}=0$) are employed on all the solid walls by setting the unknown discrete distributions equal to the values on neighboring nodes.

To solve the LB equation for the electric potential, the zeta potentials on the upper and lower walls are fixed and Dirichlet boundary conditions are employed.[33] To evaluate the electric potential at the inlet and outlet, periodic boundary conditions have been employed.

For the velocity field, we have adopted the no-slip boundary condition developed by Zou and He[34] on all the solid walls. Periodic boundary conditions are used at the channel inlet and outlet.

At the channel inlet where the sample meets the buffer, the sample is assumed to be injected over the upper half of the channel while the buffer is injected over the lower half of channel. The nondimensionalized species concentration at the inlet is therefore assumed to be unity in the upper half of the channel and zero in the lower half of the channel. A scheme using both the equilibrium distribution at the inlet nodes and the nonequilibrium part at the neighboring downstream nodes is adopted for the inlet boundary like $f_i(\text{node\_in}) = f_i^{eq}(\text{node\_in}) + (1-\delta_t/\tau)[f_i(\text{node\_in}+1) - f_i^{eq}(\text{node\_in}+1)]$. Neumann boundary conditions ($\partial c_d/\partial\mathbf{n}=0$) are implemented along the solid walls by setting the unknown discrete distributions equal to the values on neighboring nodes so that the species cannot penetrate the wall. An extrapolation scheme is used at the outlet to determine the unknown concentration distribution.

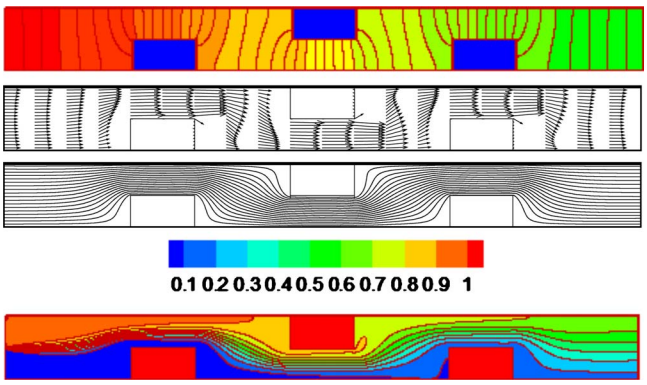

FIG. 1. (Color online) Electric potential distribution of the externally-applied electric field, velocity vectors, streamlines, and species concentration contours in the microchannel with three wall blocks. The block height $h=0.5H$ (from the top to the bottom).

III. RESULTS AND DISCUSSION

An electroosmotic flow between two parallel plates is considered. The upper and lower surfaces are defined by $y=H$ and $y=0$, the channel height is assumed to be $H=10$ μm and the channel length $L=10H$. After grid resolution test, we employed a uniform grid system of 200×2000 in the simulation. The simulated channel serves as a representative component of an integrated chip and both H and L are flexible design parameters that can easily be adjusted. Unless otherwise specified, $\varepsilon\varepsilon_0=7.79\times10^{-10}$ C^2/(J m), $T=293$ K, $e=1.6\times10^{-19}$ C, $N_A=6.02\times10^{23}$ mol^{-1}, $k_B=1.38\times10^{-23}$ J/K, $\rho=998.2$ kg/m^3, $z=+1$, $\nu=1.004\times10^{-6}$ m^2/s, the surface zeta potential, $\zeta=-100$ mV, the ionic molar concentration, $c_{inf}=10^{-5}$ mol/l, and the diffusion coefficient, $D=10^{-10}$ m^2/s, which is a general value for commonly used chemical reagents. External dc electrodes are located at the two ends of the channel and the externally-applied electric field between the channel inlet and outlet is fixed at $\Delta\phi=5$ V. Note that this fixed value sustains a uniform externally-applied electric intensity of $-\nabla\phi=50\,000$ V/m in the channel length direction for smooth channel.

A. Electroosmotic flow in microchannels patterned with rectangular blocks

To achieve a completely homogeneous solution in a relatively short channel, especially for a species with a relatively low diffusion coefficient, high mixing performance is essential. In this section, we study the effect of introducing patterned rectangular blocks of various heights and widths along the walls of the channel. The test case involves three rectangular blocks at $X=x/L=0.2-0.3$ (bottom wall), $X=0.45-0.55$ (top wall), and $X=0.7-0.8$ (bottom wall). All the blocks have a width $w=0.1L$ and a height $h=0.5H$. Figure 1 presents the electric potential distribution of the externally-applied electric field, velocity vectors, streamlines, and species concentration distribution for the case with three wall blocks. The external electric potential contours are clearly distorted by the patterned blocks. The velocity vectors and streamlines illustrate the flow disturbances created by the blocks as the bulk fluid is forced to flow through the constricted regions. However, there is no evidence of vortices or flow separation behind the blocks due to the low Reynolds number conditions associated with electroosmotic flow.

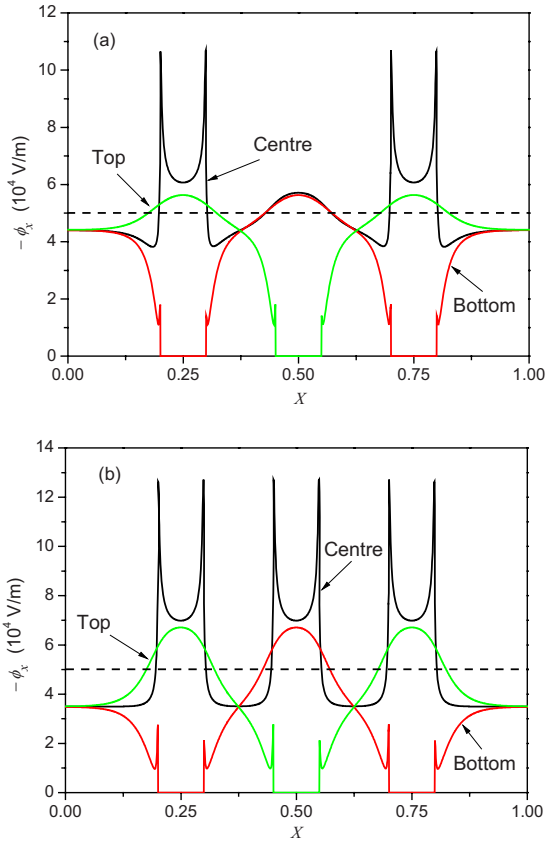

FIG. 2. (Color online) Externally-applied electric intensity distribution along the top wall, the bottom wall, and the centerline of the block channels. (a) Block channel with block height $h=0.25H$. (b) Block channel with block height $h=0.5H$.

Due to surface blocks fabricated on the channel wall, the originally uniform external electric intensity in smooth channel becomes complicated. Figure 2 presents the external electric intensity ($-\phi_x$) along the channel top wall, bottom wall, and centerline for two different block heights $h=0.25H$ [Fig. 2(a)] and $h=0.5H$ [Fig. 2(b)]. The dashed line in the figure presents the uniform distribution in smooth channel at $-\phi_x=50\,000$ V/m. From the figure we can see that the external electric intensity is still uniform at the inlet and outlet regions that are far away from the blocks, however, the magnitude is smaller than the distribution in uniform channel. The distribution varies sharply around the wall blocks. The external electric intensity is usually lower than the uniform distribution in the closest region before and after the block. However, in the regions over the bottom block and below the top block, the intensity is usually larger than the uniform distribution.

Figure 3 presents the streamwise velocity profiles across the channel at $x=0.25L$, compared with the one in smooth channel. We computed the block wall cases with ϕ_x from two different methods, one using the uniform $-\phi_x=50\,000$ V/m over all the channel and the other obtaining ϕ_x with Eq. (17) by solving the LB equation for the external

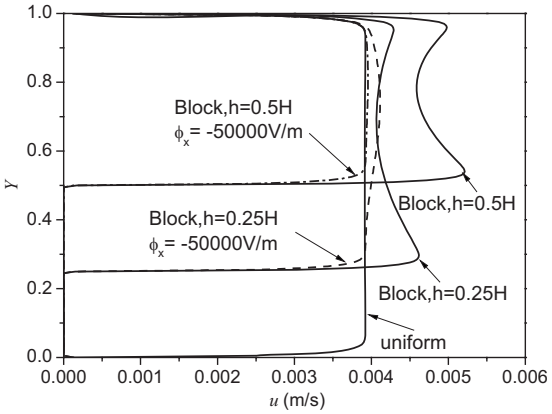

FIG. 3. Streamwise velocity profiles at $x=0.25L$ for block channels, compared with the uniform channel.

electric field. The velocity profile computed with the nonuniform ϕ_x exhibits a saddlelike shape, which results from the combination of the forward EOF and the backward pressure-driven flow. However, the velocity profile computed with uniform ϕ_x undergoes a change from a standard pluglike EOF flow in smooth channel to a parabolalike flow, which mainly owes to that the flow velocity increases suddenly due to the block constriction. For the lower block height of $h=0.25H$, the effect of the block decreases and the difference in velocity profiles becomes small between the two different computing methods. This result shows that the nonuniform distribution of the external electric field must be taken into account in complicated channels.

B. Electroosmotic flow in heterogeneous microchannels

In this section, we consider the effect of introducing a heterogeneous zeta potential along the surface of the channel. This is a commonly adopted approach for enhancing the mixing in electroosmotic flows[4–11] and can be achieved by fabricating the surface from different materials or by modifying the local surface charge, e.g., using electrodes buried beneath the substrate or through laser ablation.

The test problem consists of a smooth channel with three heterogeneous patches of $\zeta_w=+100$ mV applied along $X=0.2-0.3$ on the bottom wall, $X=0.45-0.55$ on the top wall, and $X=0.7-0.8$ on the bottom wall, while the other surfaces of the channel are maintained at a uniform zeta potential of $\zeta=-100$ mV. Figure 4 presents the velocity vectors, streamlines, and species concentration distribution for this case. In a similar manner to the wall block test case, we can clearly see the presence of flow disturbances in the heterogeneous regions. However, in this case, the velocity vectors indicate that the fluid undergoes a change in flow direction and the streamlines show local recirculation zones in the vicinity of the heterogeneous patches. In addition, the velocity profiles away from the heterogeneous regions exhibit a significant "concave" flow distribution.

Another test case investigates the use of symmetric distributions of heterogeneous patches. A surface potential of $\zeta_w=+100$ mV is applied along sections of length $0.1L$ on both the top and bottom walls at $X=0.2-0.3$, $X=0.45-0.55$, and $X=0.7-0.8$ while all the other surfaces are maintained at $\zeta=-100$ mV. Comparing Fig. 5 to Fig. 4, it can be seen that the flow patterns are quite different between the two types of zeta potential distribution. The streamlines for the asymmetric distribution of zeta potential indicate that the fluid moves through a more sinuous path compared to the symmetric distribution of zeta potential where the fluid is made to converge toward the center of the channel over the heterogeneous surface. The flow contraction and expansion effects are clearly more pronounced for the case with a symmetric zeta potential.

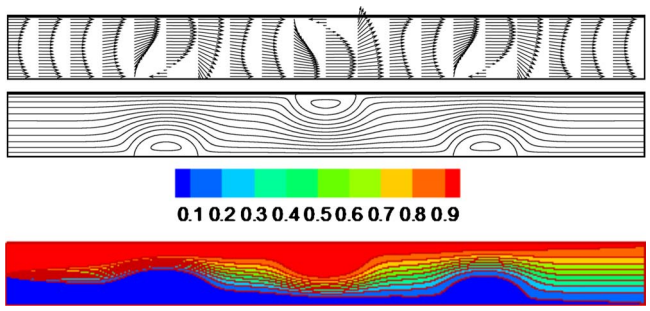

FIG. 4. (Color online) Velocity vectors, streamlines, and species concentration contours in a microchannel composed of three asymmetric sections of heterogeneous surface (from the top to the bottom).

C. Comparison of the mixing enhancement methods

Figure 6 presents the species concentration distribution across the channel ($Y=y/H$) at the channel outlet for different enhancement methods. We know that as the mixing proceeds from the channel inlet ($c_d=0$ for $0\leq Y\leq 0.5$, and $c_d=1$ for $0.5<Y\leq 1$) to the outlet, the concentration difference between the upper and lower streams becomes smaller. Since the mixing process is dominated by diffusion in the smooth channel, the present channel length is insufficient to have a homogeneously mixed sample at the outlet. From Fig. 6 we can see that all the present mixing enhancement results are effective and more approach the fully-mixed solution ($c_d=0.5$) compared to the smooth channel with uniform surface potential. For the symmetric heterogeneous potential channel and asymmetric heterogeneous potential channel, the species concentration in the upper channel and the lower channel approaches the fully-mixed solution almost at the same pace. However, for the presented block wall channels ($h=0.25H$ and $h=0.5H$), the species concentration in the upper channel

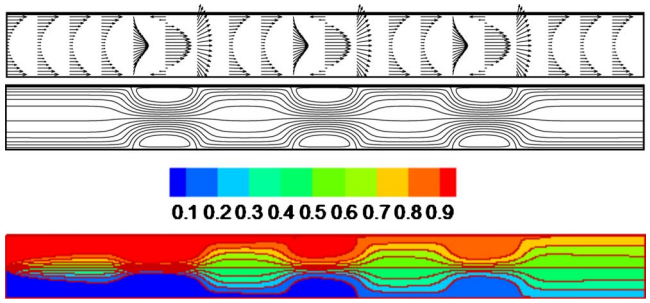

FIG. 5. (Color online) Velocity vectors, streamlines, and species concentration contours in a microchannel composed of three symmetric sections of heterogeneous surface (from the top to the bottom).

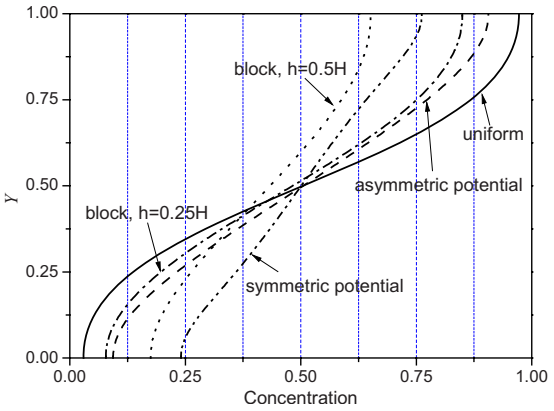

FIG. 6. (Color online) Species concentration profiles at the outlet of various mixing enhancing channels, compared with the uniform channel.

approaches the fully-mixed solution faster than the concentration in the lower channel, especially for the case of $h=0.5H$.

To quantify the mixing enhancement at the channel cross-sections along the streamwise direction, a mixing efficiency can be calculated from[10,12]

$$\sigma(x) = \left(1 - \frac{\int_0^H |c_d - c_{d,\inf}| dy}{\int_0^H |c_{d,0} - c_{d,\inf}| dy}\right) \times 100\%, \quad (22)$$

where $c_{d,0}$ and $c_{d,\inf}$ are the species concentrations in the completely unmixed ($c_{d,0}=0$ or 1) and completely mixed ($c_{d,\inf}=0.5$) states, respectively. The calculated mixing efficiency from the channel inlet to the outlet is presented in Fig. 7(a) for different enhancement methods, in comparison with the uniform channel. As the mixing proceeds, from the uniform channel it can be seen that the gradients of the mixing efficiency curves diminish due to the decreasing concentration difference between the upper and lower flow streams.

The mixing efficiency at the channel outlet is 36.3%, 50.4%, 69.1%, and 71.9% for uniform channel, asymmetric heterogeneous surface potential, block wall, and symmetric heterogeneous surface potential, respectively. The symmetric distribution of heterogeneous patches has the largest mixing efficiency. Compared with the uniform channel, the mixing efficiency at the channel outlet is improved by 38.8%, 90.4%, and 98.1% for the cases of asymmetric surface potential, wall blocks, and symmetric surface potential, respectively. It can be seen that there are two distinct minima around the block in the mixing efficiency curves for the block channel, indicating that the calculated mixing efficiency decreases in the flow contraction and expansion regions around the block. These minima are due to the definition of the mixing efficiency in Eq. (22) and have also been observed by Chang and Yang[12] and Wang *et al.*[24] The flow over the wall block increases the contact area between the fluid streams to be mixed. For the channels with heterogeneous patches, the introduction of a heterogeneous surface enhances the mixing, especially for the symmetric heterogeneous distribution.

The mixing enhancement can be attributed to the following inter-related processes: improved diffusion of the species

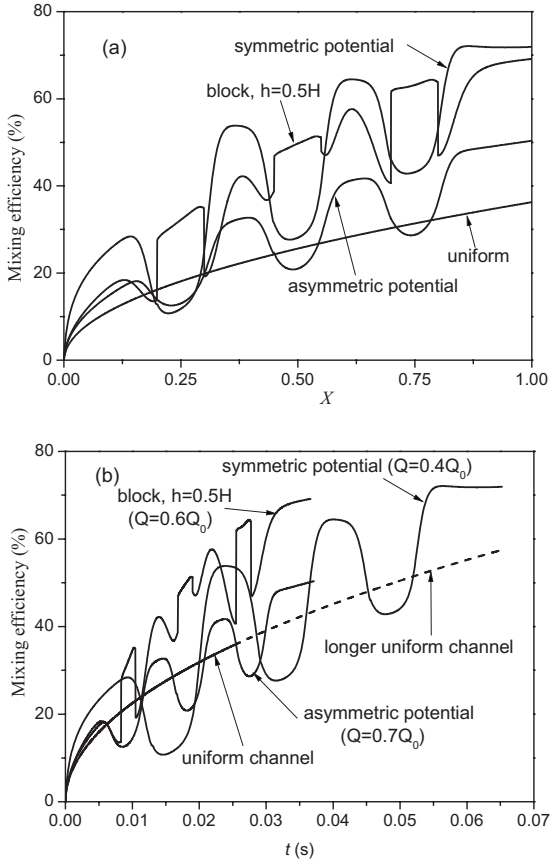

FIG. 7. Species mixing efficiency of the uniform channel, the channels with asymmetric and symmetric heterogeneous surface potentials and the channel with three wall blocks. (a) Mixing efficiency against distance. (b) Mixing efficiency against mixing time. Q is the mass flow rate and Q_0 is the mass flow rate for the uniform channel.

due to the compacted streamlines and a lower fluid velocity due to the increased flow resistance leading to a prolonged mixing time.

Previous studies have usually focused only on the mixing efficiency since this is one of the most important parameters when comparing the effectiveness of different mixing enhancement methods. However, the mixing efficiency cannot be considered in isolation since the mixing time is also an important parameter in the design of a real device. In the present study, we analyze the mixing process in terms of the mixing time, $t(x)$, for the species to travel from the inlet to position, x, along the channel. The total mixing time is the time required for a species to pass from the entrance to the exit of the microchannel. A desirable mixing enhancement method must achieve a good mixing efficiency without significantly reducing the overall flow rate.

Figure 7(b) presents the mixing efficiency against the mixing time and clearly shows the beneficial effect of introducing wall blocks or heterogeneous potential patches into the channel. In Fig. 7(b), the mass flow rate per unit width for the uniform channel is $Q_0=3.86\times10^{-5}$ kg/s. The corresponding calculated mean streamwise velocity is 0.003 86 m/s, which is in good agreement with the Helmholtz–Smoluchouski (HS) electroosmotic velocity in the standard electroosmotic flow, $u_{\mathrm{HS}}=0.003\ 89$ m/s, calculated by[35]

$$u_{\mathrm{HS}} = \frac{\varepsilon\varepsilon_0\zeta}{\mu}\nabla\phi. \tag{23}$$

where μ is the fluid dynamic viscosity. The corresponding mass flow rates for enhanced channels are indicated in Fig. 7(b) in terms of Q_0. It should be aware that the mass flow rate is reduced by introducing blockage or heterogeneous potential patches into the channel. Consequently, there is more time available for species to mix.

The mixing enhancement for the block wall, the symmetric, and asymmetric surface potentials is partly a consequence of the prolonged total mixing time due to the decreased flow rate as indicated in Fig. 7(b). It can be seen that the channel with wall blocks achieves a similar mixing efficiency to the channel with a symmetric distribution of zeta potential but in a far shorter time. We calculate that the corresponding mixing time is prolonged by 41.5%, 43.3%, and 152% for the cases of wall blocks, asymmetric surface potential, and symmetric surface potential, respectively, compared with the smooth channel. We have also tested a longer uniform channel in order to obtain a residence time comparable to the symmetric surface potential case, presented in Fig. 7(b) by a dashed line. Compared to the uniform channel with the same residence time, mixing enhancements of 15.9%, 25%, and 60.2% are achieved for the cases of asymmetric surface potential, symmetric surface potential, and three wall blocks, respectively. The wall block case is of the best effectiveness for mixing enhancement in the same mixing time. If we recall the asymmetry of the outlet concentration distribution between the upper channel and the lower channel in Fig. 6, it can also confirm that the wall block has stronger disturbance effect.

In practical applications, we usually pay more attention on the mixing enhancement without obviously reducing the flow rate. By increasing the externally-applied electric voltage, we have also obtained the mass flow rates of the enhanced cases comparable to the uniform channel. Based on the same flow rate as the magnitude in the uniform channel, the mixing efficiency at the channel outlet is 43.1%, 55.5%, and 55.6% for the cases of asymmetric surface potential, symmetric surface potential, and three wall blocks, respectively. Though the mixing efficiency for symmetric surface potential is comparable to the wall block case, the mixing time for the wall block case is reduced by 14.4% compared with the symmetric surface potential case. In addition, the applied external electric voltage for symmetric surface potential case is 1.5 times of the wall block, and 2.5 times of the uniform channel to gain the same flow rate as in the uniform channel. High externally-applied electric voltage could cause other problems in practical applications, such as Joule heating.

D. Analysis using field synergy principle

For a two-dimensional open channel flow, from the energy equation, it is deduced that the total convective heat transfer is $\int\int_S \rho c_p(\mathbf{u}\cdot\nabla T)dxdy = \int\int_S \rho c_p|\mathbf{u}|\cdot|\nabla T|\cos\theta dxdy$,[36] where c_p is the specific heat ratio. It is proved that the called synergy angle θ between the velocity field and the temperature gradient field is reduced for most of effective heat transfer enhancement methods. The analysis of the field synergy theory in enhanced heat transfer fields has matured in recent years. Be analogous to the heat transfer, we can obtain the mass transfer as

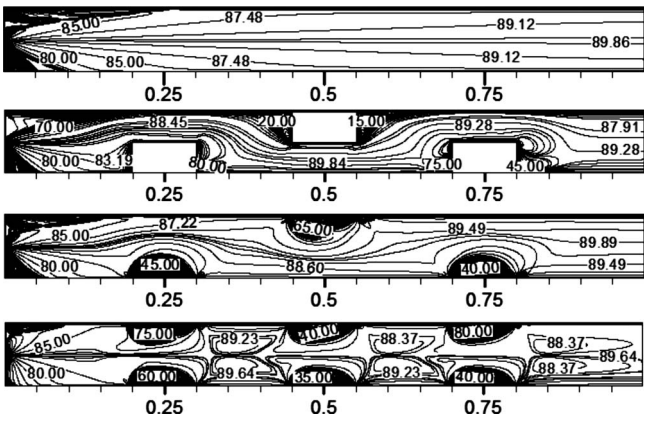

FIG. 8. Local synergy angle contours in uniform channel, block channel with block height $h=0.5H$, asymmetric heterogeneous potential channel, and symmetric heterogeneous potential channel (from the top to the bottom).

$$\int\int_S \mathbf{u}\cdot\nabla c_d dxdy = \int\int_S |\mathbf{u}|\cdot|\nabla c_d|\cos\theta dxdy, \tag{24}$$

where θ is the angle between the velocity field and the concentration gradient field. In this section, to evaluate the effectiveness of the various mixing enhancement methods, we calculate the local synergy angle via

$$\theta = \arccos\left(\frac{\mathbf{u}\cdot\nabla c_d}{|\mathbf{u}||\nabla c_d|}\right). \tag{25}$$

The calculated synergy angle is shown in Fig. 8 presented with the unit of degree. In the calculation, if an angle is larger than 90°, we replace it with its supplementary angle. For the uniform channel shown in Fig. 8(a), we can see that the synergy angle increases from the inlet to the outlet, as well as increases from the near wall region to the center zone, which means that the mixing effect is slightly higher in the inlet region and the near wall region. In the inlet region, the concentration difference in the expanse direction is very large, resulting in a better mixing effect. In the near wall region, the velocity gradient in the expanse direction is large which also results in a better mixing effect. However, the synergy angle is close to 90° in most of the channel, which denotes that the mixing effect is very weak in the whole smooth channel. For the channel patterned with rectangular blocks presented in Fig. 8(b), the synergy angle decreases largely in the regions before and after the block where the flow experiences a contraction and expansion, which shows that the mixing is enhanced by the wall blocks. For the heterogeneous channel shown in Figs. 8(c) and 8(d), the synergy angle also decreases obviously in the very near heterogeneous regions, indicating the mixing enhancement by the heterogeneous surface potential distribution. However, the synergy angle is still close to 90° in the region away from the surface block or heterogeneous patches. The authors believe that the mixing enhancement effect by the wall blocks or the

heterogeneous surface potential distribution is suppressed by the extremely small velocity in the EOF. This discussion shows that the local distribution of the synergy angle can unveil more details of the mixing enhancement process.

IV. CONCLUSIONS

Motivated by the growing interest in electroosmosis as a no-moving-component method to pump, mix, and control fluid motion in microfluidic devices, we have revisited the common mixing enhancement methods for electroosmotic flow in microchannels. The simulations have used a LB methodology to describe the external electric field, the electric potential distribution in the electrolyte, the flow field, and the species concentration.

By introducing the concept of mixing time, we have shown that the enhancement to mixing effect from the methods of wall block and heterogeneous surface zeta potential includes three aspects: the increased convection effect due to the stirring, the decreased convection effect due to the decreased velocity magnitude, and the increased molecular diffusion effect due to the prolonged mixing time.

We have shown that the introduction of wall blocks into a microchannel can significantly change the flow pattern and enhance the degree of mixing. We have also investigated the use of heterogeneous distributions of zeta potential to enhance the mixing. Although a symmetric distribution of heterogeneous zeta potential appears to be more effective than an asymmetric distribution, the observed enhancement in the mixing efficiency is mainly due to the increased total mixing time. Compared with the heterogeneous surface distribution, the wall block cases are of better mixing enhancement performance without the prolonged mixing time. Therefore, wall block channel or channel designed with complex geometry is more recommended when applying passive mixing enhancing approaches. To analyze the local diffusion mixing enhancement in the channel, we have extended the field synergy theory to the EOF. The distribution of the local synergy angle in the channel can help to understand the details of the enhancement results. Especially, by analyzing the local field synergy angle, we can precisely decide which location to distribute the enhancement scheme is most effective in a complicated system.

The present study has shown that it is important to account for the mixing time as well as the mixing efficiency when evaluating the performance of a mixing enhancing method. This is to ensure that any increase in the mixing efficiency is not mainly as a result of a longer residence time. It is therefore recommended that the assessment of mixing enhancement is best achieved by considering the mixing efficiency versus mixing time characteristics of the microchannel.

ACKNOWLEDGMENTS

The authors would like to thank the National Natural Science Foundation of China for the support under Grant No. 50776067 and the Program for NCET in university for the support under the Grant No. NCET-07-0676. G.H.T. would also like to express his grateful gratitude to Yonghao Zhang in University of Strathclyde, Xiaojun Gu, Robert W. Barber, David R. Emerson in Daresbury Laboratory, STFC, U.K. for their discussion and suggestion.

[1] D. Liepmann and J. D. Evans, Polym. Mater. Sci. Eng. Proc. ACS Div. Polym. Mater. Sci. Eng. **76**, 549 (1997).
[2] H. T. Evensen, D. R. Meldrum, and D. L. Cunningham, Rev. Sci. Instrum. **69**, 519 (1998).
[3] P. Dutta, Ph.D. thesis, Texas A&M University, 2001.
[4] C. A. Keely, T. A. A. M. van de Goor, and D. McManigil, Anal. Chem. **66**, 4236 (1994).
[5] A. Ajdari, Phys. Rev. Lett. **75**, 755 (1995).
[6] A. D. Stroock, M. Weck, D. T. Chiu, W. T. S. Huck, P. J. A. Kenis, R. F. Ismagilov, and G. M. Whitesides, Phys. Rev. Lett. **84**, 3314 (2000).
[7] A. E. Herr, J. I. Molho, J. G. Santiago, M. G. Mungal, T. W. Kenny, and M. G. Garguilo, Anal. Chem. **72**, 1053 (2000).
[8] L. Q. Ren and D. Q. Li, J. Colloid Interface Sci. **243**, 255 (2001).
[9] S. Z. Qian and H. H. Bau, Anal. Chem. **74**, 3616 (2002).
[10] D. Erickson and D. Q. Li, Langmuir **18**, 1883 (2002).
[11] L. M. Fu, J. Y. Lin, and R. J. Yang, J. Colloid Interface Sci. **258**, 266 (2003).
[12] C. C. Chang and R. J. Yang, J. Micromech. Microeng. **14**, 550 (2004).
[13] M. Sbragaglia, R. Benzi, L. Biferale, S. Succi, and F. Toschi, Phys. Rev. Lett. **97**, 204503 (2006).
[14] R. Benzi, L. Biferale, M. Sbragaglia, S. Succi, and F. Toschi, J. Fluid Mech. **548**, 257 (2006).
[15] R. Benzi, S. Succi, and M. Vergassola, Phys. Rep. **222**, 145 (1992).
[16] S. Chen and G. D. Doolen, Annu. Rev. Fluid Mech. **30**, 329 (1998).
[17] B. M. Li and D. Y. Kwok, J. Colloid Interface Sci. **263**, 144 (2003).
[18] B. M. Li and D. Y. Kwok, J. Chem. Phys. **120**, 947 (2004).
[19] S. Melchionna and S. Succi, J. Chem. Phys. **120**, 4492 (2004).
[20] F. Z. Tian and D. Y. Kwok, Langmuir **21**, 2192 (2005).
[21] Z. L. Guo, T. S. Zhao, and Y. Shi, J. Chem. Phys. **122**, 144907 (2005).
[22] J. K. Wang, M. Wang, and Z. X. Li, J. Colloid Interface Sci. **296**, 729 (2006).
[23] G. H. Tang, Z. Li, J. K. Wang, Y. L. He, and W. Q. Tao, J. Appl. Phys. **100**, 094908 (2006).
[24] D. N. Wang, J. Summers, and P. H. Gaskell, Nanoscale Microscale Thermophys. Eng. **11**, 1 (2007).
[25] Z. H. Chai, Z. L. Guo, and B. C. Shi, J. Appl. Phys. **101**, 104913 (2007).
[26] D. A. Kanti, A. Mukhopadhyay, and I. K. Puri, Microfluid. Nanofluid. **4**, 463 (2008).
[27] X. Y. He and L. S. Luo, Phys. Rev. E **56**, 6811 (1997).
[28] Y. H. Qian, D. d'Humieres, and P. Lallemand, Europhys. Lett. **17**, 479 (1992).
[29] N. A. Patankar and H. H. Hu, Anal. Chem. **70**, 1870 (1998).
[30] J. Santiago, Anal. Chem. **73**, 2353 (2001).
[31] L. Q. Ren and D. Q. Li, Anal. Chim. Acta **531**, 15 (2005).
[32] X. Y. He and N. Li, Comput. Phys. Commun. **129**, 158 (2000).
[33] G. H. Tang, W. Q. Tao, and Y. L. He, Phys. Rev. E **72**, 016703 (2005).
[34] Q. Zou and X. Y. He, Phys. Fluids **9**, 1591 (1997).
[35] R. J. Hunter, *Zeta Potential in Colloid Science* (Academic, London, 1981).
[36] W. Q. Tao, Z. Y. Guo, and B. X. Wang, Int. J. Heat Mass Transfer **45**, 3849 (2002).